Journal of Sound and Vibration (2001) **240**(1), 131–157
doi:10.1006/jsvi.2000.3198, available online at http://www.idealibrary.com on IDEAL®

MOTION OF A MOVING ELASTIC BEAM CARRYING A MOVING MASS—ANALYSIS AND EXPERIMENTAL VERIFICATION

S. PARK

Mechatronics Research Team, Research Institute of Industrial Science and Technology (RIST), San 32, Hyoja-dong, Nam-ku, 790-330, Pohang, Korea. E-mail: sdpark@rist.re.kr

AND

Y. YOUM

Robotics and Bio-Mechatronics Laboratory, School of Mechanical Engineering, Pohang University of Science and Technology (POSTECH), San 31, Hyoja-dong, Nam-ku, 790-784, Pohang, Korea. E-mail: youm@postech.ac.kr

(*Received* 23 *March* 2000, *and in final form* 10 *July* 2000)

In this paper, vibrational motion of an elastic beam fixed on a moving cart and carrying a moving mass is investigated. The equations of motion of the beam–mass–cart system are derived and the coupled dynamic equations are solved by the unconstrained modal analysis. In modal analysis, the exact normal mode solutions corresponding to the eigenfrequencies for each position of the moving mass and the ratios of the weight of the beam–mass–cart system are used. Proper transformation of time solutions between the normal modes for a position and those for the next position of the moving mass is also considered. Numerical simulations are carried out to obtain open-loop responses of the system in tracking pre-designed paths of the moving mass. The simulation results show that the model predicts the dynamic behavior of the beam–mass–cart system well. Experiments are carried out to show the validity of the proposed analytical method.

1. INTRODUCTION

In the past, a lot of research work has been reported on dynamic analysis of an elastic beam with a moving force or mass. Initially, the problem of moving mass load on an elastic beam is originated mainly from the applications in the field of transportation such as bridges, railways and guide ways supporting a moving mass load.

As the historical review of the latter half of last century, Ayre *et al.* [1] studied the effect of the ratio of the weight of the load to the weight of a simply supported beam for a constantly moving mass load. They also obtained the exact solution for the resulting partial differential equation by using the infinite series. Kenney [2] found the possible velocities for the propagation of free bending waves and studied their relation to the critical velocity of the beam. He also presented an analytic solution and resonance diagrams for a constant velocity of a rapidly moving load on an elastic foundation including the effect of viscous damping. Steele [3] investigated the series solution of a finite, simply supported Euler–Bernoulli beam, with and without an elastic foundation. Nelson and Conover [4] analyzed the dynamic stability of the lateral response of a simply supported Bernoulli–Euler beam carrying a continuous series of equally spaced mass particles. Stanišić and Hardin [5]

0022-460X/01/060131 + 27 $35.00/0

developed a theory describing the response of a beam under an arbitrary number of moving masses by using Fourier finite sine transforms. Ting *et al.* [6] developed an algorithm to solve the dynamic response of a finite elastic beam supporting a constantly moving mass.

Relevant to the research works after 1990s, Olsson [7] presented analytical and finite element solutions to the dynamic problem of a simply supported beam subjected to a constant force moving at a constant speed. Mackertich [8] presented the response of a beam to a constant moving mass utilizing the beam theory with corrections for the shear deformation and rotary inertia. Lee [9] formulated the equation of motion for an Euler beam acted upon by a concentrated mass moving at a constant speed by using the Lagrangian approach and the assumed mode method. He also pointed out the possibility of the mass separation from the beam during the course of the motion by monitoring the contact forces between the mass and the beam. Lee [10] investigated the onset of the separation between the moving mass and the beam while taking account of its effect in calculating the interact force and the dynamic responses of the beams. Foda and Abduljabbar [11] presented an exact and direct modelling technique based on the dynamic Green function for the modelling beam structures subjected to a mass movement at constant speed.

All the above works dealt with simply supported or cantilevered beams with constantly moving masses or forces because the main purpose of those works was the vibration analysis of bridges, railroads or guide ways on which the moving mass load or force passes. However, when an elastic beam carrying a moving mass, is fixed on a moving cart movement with the dynamical and if the total mass of the beam and the moving mass cannot be neglected with respect to that of the cart, then the motion of the beam-mass system affects that of the cart, and vice versa. Therefore, in this case, the dynamic equations for the beam–mass–cart system should be considered as a whole.

For example, when the reclaimers in automatic warehouses, high tower cranes, ladder cars or overhead cranes move a heavy load, the vibrational motions due to the flexibility of the main beam are unavoidable. Furthermore, when the load moves along the flexible beam, the vibrational motions vary along the position of the load as that of the ratios of the weight of the beam–mass–cart system [12]. Therefore, to analyze the total motion of the beam–mass–cart system, the rigid-body motion of the cart as well as the vibrational motion of the beam-mass system should be included in the analysis.

In this paper, the motion of a Bernoulli–Euler beam fixed on a moving cart and carrying a moving mass along the beam is analyzed. The differences, both in modelling and analysis, between the previous works and this one are: (1) The flexible beam considered here is fixed on a moving cart. That is, it is not restrained at a large reference frame. Therefore, in the mathematical modelling to derive the equations of motion, the total dynamics of the beam-mass-cart system is considered. (2) The velocities of the moving mass and the cart are not constants. (3) At every position of the moving mass, the exact normal mode solutions corresponding to the eigenfrequencies of the beam–mass–cart system are used to solve the equation of motion. (4) Proper transformations of the time solutions between normal modes for a position and those for the next position of the moving mass are adopted.

In the following section the equation of motion of the beam–mass–cart system is derived, and the modal analysis is described in section 3. Numerical simulations for the open-loop responses of the system in tracking the pre-designed path of the moving mass are performed in section 4, some experimental results are introduced in section 5, followed by conclusions.

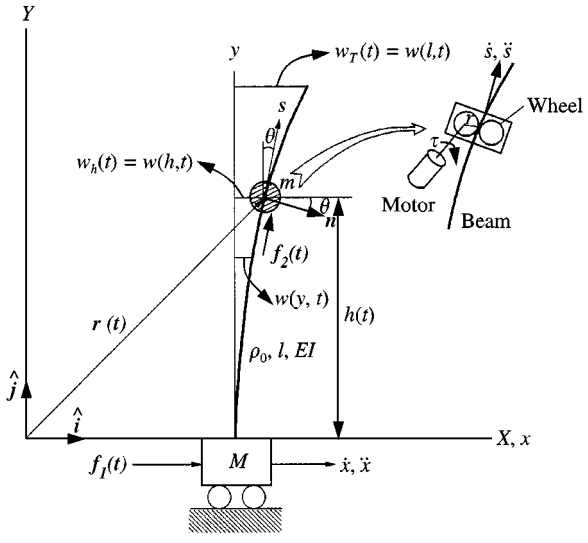

Figure 1. The beam-mass-cart system considered.

2. MATHEMATICAL MODELLING

Figure 1 shows a Bernoulli–Euler beam fixed on a moving cart, carrying a moving mass. The base cart moves on the horizontal plane by the applied force $\mathbf{f}_1(t)$. The moving mass moves along the beam by the friction wheels driven by a motor.

To derive the equations of motion of the beam–mass–cart system, the following assumptions are made: (1) The driving force for the cart, $\mathbf{f}_1(t)$, is applied to $\hat{\mathbf{i}}$ direction. (2) The local driving force for the moving mass, $\mathbf{f}_2(t) = \tau(t)r$, where $\tau(t)$ is the torque by the driving motor of the moving mass and r is the radius of the driving wheel of the moving mass, is generated by the driving motor of the moving mass and makes the moving mass to move to the tangential direction of the deformed beam. (3) The moving mass is not separated from the beam. (4) There is no longitudinal deflection of the beam and only the lateral deflection is possible. (5) The lateral deflection of the beam is small compared with the length of the beam. (6) The rotational effect of the moving mass and the beam with respect to the local co-ordinate system is neglected. (7) All the motion occurs in XY plane, and overturn motion of the system does not occur.

Under these assumptions, at any time t, if the magnitudes of tangential velocity and acceleration of the moving mass are $\dot{s}$ and $\ddot{s}$, respectively, and the vertical position of the moving mass is $h(t)$, then the velocity of the moving mass with respect to the reference co-ordinate system is represented as

$$\dot{\mathbf{r}}(t) = (\dot{x} + \dot{w}_h + \dot{s}\sin\theta)\hat{\mathbf{i}} + \dot{s}\cos\theta\hat{\mathbf{j}}, \tag{1}$$

where $w_h = w(h(t), t)$ is the deflection of the flexible beam at $y = h(t)$ and

$$\tan\theta = \left.\frac{\partial w(y,t)}{\partial y}\right|_{y=h(t)}. \tag{2}$$

The mass per unit length of the flexible beam with a moving mass m at height $h(t)$ along the beam can be represented as

$$\rho = \rho_0 + m\delta[y - h(t)], \tag{3}$$

where ρ_0 is the mass per unit length of the flexible beam without the moving mass, m is the mass of the moving mass, and $\delta[y - h(t)]$ is the *delta-function* satisfying

$$\int_0^l \delta[y - h(t)]\,\mathrm{d}y = 1. \tag{4}$$

The kinetic energy, $K(t)$, and the potential energy, $P(t)$, of the cart and the flexible beam with a moving mass located at $h(t)$ are represented as

$$\begin{aligned} K(t) &= K_r(t) + \int_0^l K_e(y, t)\,\mathrm{d}y, \\ P(t) &= P_r(t) + \int_0^l P_e(y, t)\,\mathrm{d}y, \end{aligned} \tag{5}$$

where $K_r(t)$ and $P_r(t)$ are the kinetic and the potential energy functions due to the motion of the cart, and $K_e(y, t)$ and $P_e(y, t)$ are the kinetic and the potential energy density functionals due to the flexibility of the beam, respectively, and are represented, utilizing equation (1), as follows:

$$\begin{aligned} K_r &= \tfrac{1}{2} M\dot{x}^2, \\ K_e &= \tfrac{1}{2}[\rho_0 + m\delta(y - h)](\dot{x} + \dot{w})^2 + \tfrac{1}{2} m\delta(y - h)[\dot{s}^2 + 2\dot{s}\sin\theta(\dot{x} + \dot{w})], \\ P_r &= 0, \\ P_e &= \tfrac{1}{2} EI(w'')^2 + m\delta(y - h)gh, \end{aligned} \tag{6}$$

where M is the mass of the cart, EI is the flexural rigidity of the beam, $\dot{w} = \partial w(y, t)/\partial t$ and $w'' = \partial^2 w(y, t)/\partial y^2$ where $w(y, t)$ is the deflection of the beam at y.

The equations of motion can be obtained from Hamilton's principle as follows:

$$\int_{t_1}^{t_2} \left\{ \delta L_r(t) + \int_0^l \delta L_e(y, t)\,\mathrm{d}y + \delta W_{nc}(t) \right\} \mathrm{d}t = 0, \tag{7}$$

where W_{nc} is the work done by non-conservative forces, $L_r = K_r - P_r$, and $L_e = K_e - P_e$.

From Figure 1, it can be easily seen that

$$\dot{h} = \dot{s}\cos\theta. \tag{8}$$

Thus, from equations (6) and (8), it can be seen that

$$L_r = \tfrac{1}{2} M\dot{x} = L_r(\dot{x}), \tag{9}$$

and

$$\begin{aligned} L_e &= \tfrac{1}{2}[\rho_0 + m\delta(y - h)](\dot{x} + \dot{w})^2 + \tfrac{1}{2} m\delta(y - h)\{\dot{h}^2[1 + (w')^2] + 2\dot{h}w'(\dot{x} + \dot{w})\} \\ &\quad - \tfrac{1}{2} EI(w'')^2 - m\delta(y - h)gh \\ &= L_e(\dot{x}, \dot{w}, w', w'', \dot{h}, h). \end{aligned} \tag{10}$$

Since $\mathbf{f}_2(t)$ is not a global force but a local force, the virtual work done by all the nonservative forces, $\delta W_{nc}(t)$, is given by

$$\delta W_{nc}(t) = f_1(t)\delta x + f_2(t)\delta s = f_1(t)\delta x + \frac{f_2(t)}{\cos\theta}\delta h, \tag{11}$$

where δs is the virtual displacement to s direction.

The equations of motion and the boundary conditions are obtained as follows by substituting equations (8)–(11) into equation (7), integrating the resulted equation by parts and considering that the time t_1 and t_2 are arbitrary and that δx, δh and δw are arbitrary and independent [13, 14] (see Appendix A).

$$M\ddot{x} + \int_0^l \{[\rho_0 + m\delta(y-h)](\ddot{x} + \ddot{w}) + m\delta(y-h)[\ddot{h}w' + 2\dot{h}\dot{w}' + \dot{h}w'']\}\,\mathrm{d}y = f_1(t), \quad (12)$$

$$EIw'''' + [\rho_0 + m\delta(y-h)](\ddot{x} + \ddot{w}) + m\delta(y-h)[\ddot{h}w' + 2\dot{h}\dot{w}' + \dot{h}^2w''] = 0, \quad (13)$$

$$m\{\ddot{h}[1 + (w_h')^2] + (\ddot{x} + \ddot{w}_h + \dot{h}^2w_h'' + 2\dot{h}\dot{w}_h')w_h' + g\} = \frac{f_2(t)}{\cos\theta} \quad (14)$$

and

$$w(0,t) = w'(0,t) = w''(l,t) = w'''(l,t) = 0. \quad (15)$$

For small θ, equation (14) can be rewritten as

$$m\{\ddot{h} + (\ddot{x} + \ddot{w}_h + \dot{h}^2w_h'' + 2\dot{h}\dot{w}_h')w_h' + g\} = f_2(t). \quad (16)$$

since $\sin\theta \approx \tan\theta = w_h'$, $1 + (w_h')^2 = \sec^2\theta \approx 1$, and $\cos\theta \approx 1$ for small θ.

Equation (12) contains x directional inertial force of the beam–mass–cart system, the inertial forces of the beam and the mass due to the deflection of the beam and those by linear, Coriolis and centripetal accelerations of the moving mass. Equation (13) is exactly the same as the results in references [6, 9, 10, 15, 16] except the x directional acceleration term of the loaded beam. Equation (16) describes the motion of the moving mass by the applied force, $\mathbf{f}_2(t)$, and by the motion of the elastic beam. In this study the coupled equations (12), (13) and (16) are solved simultaneously utilizing the *unconstrained modal analysis* [17, 18] in the next section assuming that the vertical position of the moving mass is pre-designed.

3. MODAL ANALYSIS

To solve the partial differential equations like equation (13), some investigators used influence functions or Green functions [6, 10, 11], sine series [5, 7, 19] or assumed mode functions [9]. In separating the deflection of an elastic beam into time solutions and mode solutions, many authors used the normal modes of the beam without the moving mass (see, for example reference [9, 10]). However, the normal mode functions used in above works do not represent the exact mode solutions because the natural frequencies and the corresponding normal mode solutions of the beam are changed as the position of the concentrated mass changes [12].

When one tries to solve the coupled equations of motion utilizing modal analysis, it is impossible to separate the variables of the elastic deflection of the beam by proper mode functions and time functions because the vibration characteristics of a beam with a moving mass changes along the position of the mass while the method of separation of variables is focussed on the constant link lengths. Examples of this kind of system can be seen in references [20, 21].

In this approach, to solve the coupled equations of motion using unconstrained modal analysis, exact normal mode solutions corresponding to the frequency characteristics for

the position of the moving mass and the weight ratios of the beam–mass–cart system are used under the following assumptions.

Assumption. (1) If the magnitudes of the vertical velocity and acceleration of the moving mass are small as $\dot{\bar{h}}/l \ll \omega_{fund}$ and $\ddot{\bar{h}}/l \ll \omega_{fund}^2$, where ω_{fund} is the fundamental frequency of the beam–mass–cart system, then, at a certain time t, the moving mass is considered to be fixed at $\bar{h}$ during a small time interval Δt while $\dot{h}$ and $\ddot{h}$ are still valid. (2) The beam oscillates in the same manner during this time interval.

In the above assumptions, $\dot{\bar{h}}/l \ll \omega_{fund}$ and $\ddot{\bar{h}}/l \ll \omega_{fund}^2$ are reasonable in many industrial applications because the speed of the moving mass is relatively small compared to the vibration frequency of the beam. Under these assumptions, we can find the natural frequencies and corresponding normal mode solutions for the system which has a fixed mass at an arbitrary position $\bar{h}^o$. Then, we solve the original equations of motion several times utilizing these mode solutions during $\bar{h}^o \leqslant h(t) < \bar{h}^o + \Delta h$ while updating $\dot{h}(t)$ and $\ddot{h}(t)$ at every Δt. If $h(t) \geqslant \bar{h}^o + \Delta h = \bar{h}^n$, we find new natural frequencies and the corresponding normal modes with new position of the moving mass, $\bar{h}^n$. Then, we solve the original equations of motion again utilizing these updated mode solutions and proper transformation of time solution during $\bar{h}^n \leqslant h(t) < \bar{h}^n + \Delta h$.

The equations of motion for the beam–mass–cart system which has a fixed mass at $\bar{h}$ are given as follows:

$$M\ddot{x} + \int_0^l [\rho_0 + m\delta(y - \bar{h})](\ddot{x} + \ddot{w})\,\mathrm{d}y = f_1(t), \tag{17}$$

$$EIw'''' + [\rho_0 + m\delta(y - \bar{h})](\ddot{x} + \ddot{w}) = 0, \tag{18}$$

and the boundary conditions of equation (15).

By *unconstrained modal analysis*, the deflection of the beam at y, $w(y, t)$, and the position of the cart, $x(t)$, can be represented, respectively, as [17, 18]

$$w(y, t) = \sum_{i=1}^{\infty} \phi_i(y) q_i(t) \tag{19}$$

and

$$x(t) = \alpha(t) + \sum_{i=1}^{\infty} \beta_i q_i(t), \tag{20}$$

where $\alpha(t)$ describes the motion of the center of mass of the total system without perturbation, and

$$\phi_i(y) = \psi_i(y) - \beta_i, \tag{21}$$

where

$$\psi_i(y) = \left[A_i(y) + \frac{C_i}{1 - D_i} B_i(y) \right] \psi_i(\bar{h}) \triangleq F_i(y)\psi_i(\bar{h}) \tag{22}$$

and

$$\beta_i = -\frac{m}{M}\psi_i(\bar{h}) - \frac{\rho_0}{M}\int_0^l \psi_i(y)\,\mathrm{d}y, \tag{23}$$

where $A_i(y)$, $B_i(y)$, C_i, D_i and $\psi_i(\bar{h})$ for each eigenvalue k_i are given in Appendix B. The eigenvalues k_i are the roots of the frequency equation [12]

$$\begin{aligned}
&1 + \cos\xi\cosh\xi \\
&+ \frac{r_1}{4}[\cos\xi\cosh(\xi - 2\eta) + \cos\{\xi - 2\eta)\cosh\xi + \sin\xi\sinh(\xi - 2\eta) \\
&\qquad - \sin(\xi - 2\eta)\sinh\xi + 2\cos\xi\cosh\xi + 4\cos\eta\cosh\eta] \\
&+ \frac{r_2}{\xi}(\sin\xi\cosh\xi + \cos\xi\sinh\xi) \\
&+ \frac{r_3\xi}{4}[2\sin(\xi - \eta)\cosh(\xi - \eta) - 2\cos(\xi - \eta)\sinh(\xi - \eta) \\
&\qquad + 2\cos\eta\sinh\eta - 2\sin\eta\cosh\eta + \cos(\xi - 2\eta)\sinh\xi \\
&\qquad - \sin\xi\cosh(\xi - 2\eta) + \cos\xi\sinh\xi - \sin\xi\cosh\xi] = 0,
\end{aligned} \tag{24}$$

where $r_1 = m/M$, $r_2 = m_b/M$, $r_3 = m/m_b$, $\xi = kl$ and $\eta = k\bar{h}$. Using the normal mode solution in equation (21) we solve equations (12), (13) and (16) during $\bar{h} \leqslant h(t) < \bar{h} + \Delta h$.

If equation (23) is satisfied, the motion of the center of mass when $h(t) = \bar{h}$ is obtained as

$$M_t\ddot{\alpha}(t) + m\left[\ddot{h}(t)\sum_{i=1}^{\infty}\phi_i'(\bar{h})q_i(t) + 2\dot{h}(t)\sum_{i=1}^{\infty}\phi_i'(\bar{h})\dot{q}_i(t) + \dot{h}^2(t)\sum_{i=1}^{\infty}\phi_i''(\bar{h})q_i(t)\right] = f_1(t), \tag{25}$$

where $M_t = M + m + m_b$ is the total mass of the cart–beam–mass and $m_b = \rho_0 l$ is the mass of the flexible beam.

On the other hand, $\psi_i(y)$ in equations (21) and (22) satisfies [12]

$$EI\psi_i''''(y) - \omega_i^2\bar{\rho}\psi_i(y) = 0, \tag{26}$$

and

$$\int_0^l \bar{\rho}\phi_i(y)\psi_j(y) = \delta_{ij}, \tag{27}$$

where

$$\omega_i^2 = \frac{EIk_i^4}{\rho_0}, \tag{28}$$

$\bar{\rho} = \rho_0 + m\delta(y - \bar{h})$ and δ_{ij} is the *Kronecker delta*. Substituting equations (19), (20) and (26) into equation (13), multiplying both sides of the resulted equation by $\phi_j(y)$, integrating over the problem domain and applying the orthogonality condition as equation (27), one obtains

$$\begin{aligned}
\ddot{q}_i(t) + \omega_i^2 q_i(t) + m\Bigg[&\ddot{h}(t)\sum_{j=1}^{\infty}\int_0^l \delta(y - \bar{h})\phi_j'(y)\phi_i(y)q_j(t)\,\mathrm{d}y \\
&+ 2\dot{h}(t)\sum_{j=1}^{\infty}\int_0^l \delta(y - \bar{h})\phi_j'(y)\phi_i(y)\dot{q}_j(t)\,\mathrm{d}y \\
&+ \dot{h}^2(t)\sum_{j=1}^{\infty}\int_0^l \delta(y - \bar{h})\phi_j''(y)\phi_i(y)\dot{q}_j(t)\,\mathrm{d}y\Bigg] = \ddot{\alpha}(t)M_t\beta_i.
\end{aligned} \tag{29}$$

Substitution of equation (25) into equation (29) gives

$$\ddot{q}_i(t) + \omega_i^2 q_i(t) + m\psi_i(\bar{h})\left[\ddot{h}(t)\sum_{j=1}^{\infty}\phi_j'(\bar{h})q_j(t) + 2\dot{h}(t)\sum_{j=1}^{\infty}\phi_j'(\bar{h})\dot{q}_j(t) + \dot{h}^2(t)\sum_{j=1}^{\infty}\phi_j''(\bar{h})q_j(t)\right] = \beta_i f_i(t). \tag{30}$$

Equation (30) is the one to find the time solution for the moving mass located at $\bar{h} \leqslant h(t) < \bar{h} + \Delta h$. If the position of the mass is changed sufficiently large enough that it must be updated, then the natural frequencies and the corresponding normal modes for the position $\bar{h}$ are no longer valid. In this case, we should find new natural frequencies and the corresponding normal modes with updated position of the moving mass. Then we solve the original equations of motion and the time solutions, equation (30), again using the updated mode solutions.

However, in calculating the time solutions with new mode solutions, there must be proper transformations between old time solutions and new ones. If the position of the moving mass is changed from $\bar{h}^o$ to $\bar{h}^n + \Delta h$ at any time instant t, then the deflection of the beam at this time can be represented by using either $\bar{h}^o$ or $\bar{h}^n$ as follows:

$$w(y, t) = \sum_{i=1}^{\infty} q_i^o(t)\phi_i^o(y) = \sum_{j=1}^{\infty} q_j^n(t)\phi_j^n(y), \tag{31}$$

where $\phi_i^o(y)$ and $\phi_j^n(y)$ are the normal mode solutions corresponding to the eigenfrequencies for the position $\bar{h}^o$ and $\bar{h}^n$ respectively. The error between the two expressions in equation (31) will be checked in the next section.

Multiplying both sides of equation (31) by $\bar{\rho}^n\psi_j^n(y)$, integrating over the problem domain and applying the orthogonality condition, equation (27), one can obtain the transformation between old time solutions and new ones as follows:

$$q_j^n(t) = \sum_{i=1}^{\infty} q_i^o(t)\int_0^l \bar{\rho}^n(y)\phi_i^o(y)\psi_j^n(y)\,\mathrm{d}y, \tag{32}$$

where $\bar{\rho}^n = \rho_0 + m\delta(y - \bar{h}^n)$. Equation (32) is used to transform the time solutions when the natural frequencies and the corresponding mode solutions for $\bar{h}_o$ are changed to those for $\bar{h}^n$.

For numerical simulations, *finite-dimensional* approximated model for a finite number of mode solutions are considered from the previous development by taking the first ρ expansion in equations (19) and (20) as follows:

$$w(y, t) = \sum_{i=1}^{p} \phi_i(y)q_i(t), \tag{33}$$

and

$$x(t) = \alpha(t) + \sum_{i=1}^{p} \beta_i q_i(t), \tag{34}$$

respectively, and the results are shown in the next section.

4. NUMERICAL EXAMPLES

4.1. LINEAR MOTION OF MOVING MASS

Numerical simulations are carried out to obtain open-loop responses of the beam–mass–cart system when the moving mass follows pre-designed paths by several ways.

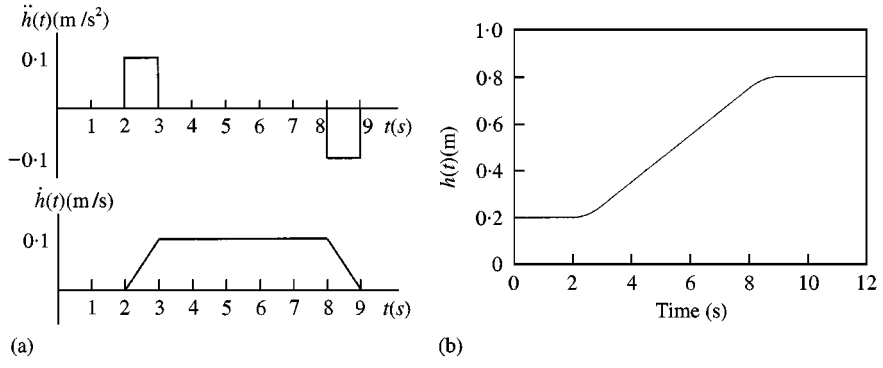

Figure 2. The acceleration, velocity and position profiles of the moving mass for upward motion: (a) acceleration and velocity profiles of the moving mass; (b) position profile of the moving mass.

At first, the forcing function $f_1(t)$ given by

$$f_1(t) = \begin{cases} 20N & \text{when } 0 < t \leqslant 0{\cdot}2, \\ -20N & \text{when } 1{\cdot}0 < t \leqslant 1{\cdot}2, \\ N & \text{otherwise} \end{cases} \tag{35}$$

is applied to the cart while $f_2(t)$ is pre-designed to generate the trajectory of the moving mass as given in Figure 2.

Figure 3 shows the position of the cart, $x(t)$, the global position of the moving mass, $x_h(t)$, the global position of the tip of the elastic beam, $x_T(t)$, the local deflection of the beam at which the moving mass is located, $w_h(t)$, and the local deflection of the beam at the tip of the beam, $w_T(t)$, respectively, where $x_h(t) = x(t) + w_h(t)$ and $x_T(t) = x(t) + w_T(t)$, when $m = 2kg$, $\Delta h = l/200$, $p = 3$ and the system parameters given in Table 1 are used.

As seen in Figure 3, the deflection at $y = h$, $w_h(t)$, becomes large as the moving mass moves from $h = 0{\cdot}2$ to $0{\cdot}8$ while the tip deflection, $w_T(t)$, at steady state is bounded within $\pm 0{\cdot}031(m)$. It can be also known that the motion of the vibrating beam and the moving mass affects that of the cart, and vice versa. Furthermore, the natural frequency of the beam gets low as the position of the moving mass becomes high. The change of the fundamental frequency during this motion by equation (28) is from 2·106 Hz (13·23 rad/s) to 0·914 Hz (5·74 rad/s), and the conditions that $\dot{h}/l \ll \omega_{fund}$ and $\ddot{h}/l \ll \omega_{fund}^2$ in the assumption are sufficiently satisfied since $\dot{h}_{max} = 0{\cdot}1$ m/s, $\ddot{h}_{max} = 0{\cdot}1$ m/s^2 and $h = 1$ m in this simulation.

In the numerical simulations, Δt is given as $\Delta t = 2\pi/100\omega_{fund}$, and, thus Δt varies from $4{\cdot}74 \times 10^{-3}$ to $10{\cdot}95 \times 10^{-3}$ s while the moving mass moves from $h = 0{\cdot}2$ to $h = 0{\cdot}8$ m. If the moving mass moves with the maximum velocity, the moving mass can move from minimum 0·474 mm to maximum 1·095 mm during Δt. Therefore, the assumption that the moving mass is fixed at a certain position during Δt is valid. In this numerical simulation, the natural frequencies are updated at every $\Delta h = l/200 = 5$ mm. In which case, for example, the fundamental frequency at $h = 0{\cdot}8$ and $0{\cdot}795$ m are 0·914 and 0·922 Hz respectively. Thus, the difference of fundamental frequencies between $h = 0{\cdot}8$ and $0{\cdot}795$ m is negligible. Furthermore, when the moving mass moves from $h = 0{\cdot}795$ to $0{\cdot}8$ m with the maximum velocity, it takes 0·05 s $= 5{\cdot}422\Delta t$. Therefore, the assumption that the beam oscillates in the same manner during Δt is valid.

TABLE 1

System parameters

Parameters	Value
Mass of cart, M	10·0 kg
Length of elastic beam, l	1·0 m
Mass per unit length of elastic beam, ρ_0	0·788 kg/m
Young's modulus of elastic beam, E	$2{\cdot}07 \times 10^{11}$ N/m^2
Area moment of inertia of elastic beam, I	$5{\cdot}208 \times 10^{-11}$ m^4

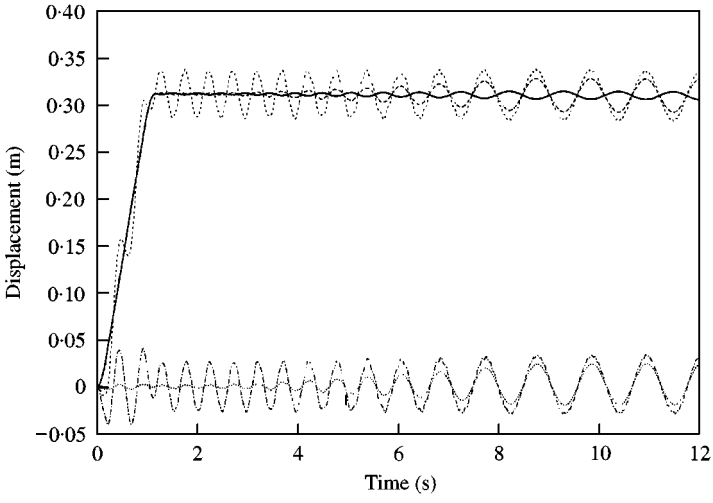

Figure 3. The open-loop response of the beam-mass-cart system by the forcing function (35) and the trajectory of moving mass in Figure 2 when $m = 2$ kg: (—), $x(t)$; (– –), $x_h(t)$; (- - -), $x_T(t)$; (· · ·), w_h; (– · –), $w_T(t)$.

Figure 4 shows the drastic change of the first three roots of the frequency equation (24) and the selected corresponding mode shapes with respect to the change of the position of the moving mass, and that is the reason why the normal mode solutions should be updated at every position of the moving mass.

Figure 5 shows the open-loop response of the beam–mass–cart system when the same parameters and conditions in the previous simulations are used except that $m = 5$ kg. The tip deflection, $w_T(t)$, at steady state is bounded within $\pm 0{\cdot}05(m)$. The fundamental frequency of the system by equations (28) and (24) is changed from 2·093 to 0·675 Hz as the moving mass moves from 0·2 to 0·8 m.

The vibrational motion of the beam–mass–cart system when the moving mass moves down from high position to lower one was investigated. For this purpose, the acceleration, velocity and position profile of the moving mass was pre-designed as seen in Figure 6.

Figures 7 and 8 show the downward open-loop responses of the beam–mass–cart system when $m = 2$ and 5 kg respectively. As seen in both figures, the frequency of the system vibration becomes higher and w_h becomes smaller as the moving mass goes down. Both results show that the tip deflections are bounded within $\pm 0{\cdot}042(m)$ and $\pm 0.173(m)$ when $m = 2$ and 5 kg, respectively, while w_h becomes smaller as the moving mass goes downward.

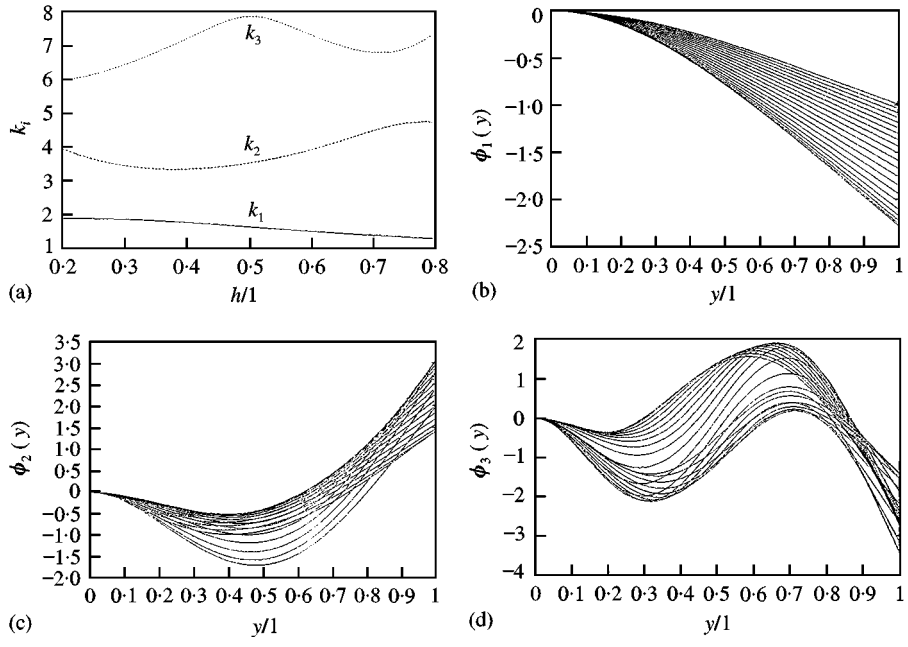

Figure 4. The first three roots of the frequency equation (24) and the selected corresponding mode shapes with respect to the change of the position of the moving mass when $m = 2$ kg: (a) the eigenfrequencies; (b) the first mode shapes; (c) the second mode shapes; (d) the third mode shapes.

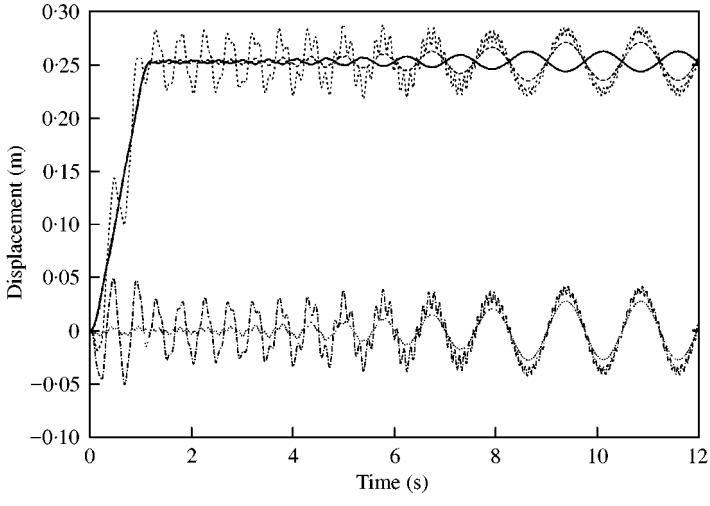

Figure 5. The open-loop responses of the beam-mass-cart system by the forcing function (35) and the trajectory of moving mass in Figure 2 when $m = 5$ kg: (—), $x(t)$; (– –), $x_h(t)$; (- - -), $x_T(t)$; (· · ·), w_h; (– · –), $w_T(t)$.

4.2. CIRCULAR MOTION OF MOVING MASS

Next numerical simulation are carried out to obtain the open loop responses of the system in tracking the pre-designed path of the moving mass. The task is to draw a circle

$$(X - x_c)^2 + (Y - y_c)^2 = R^2 \tag{36}$$

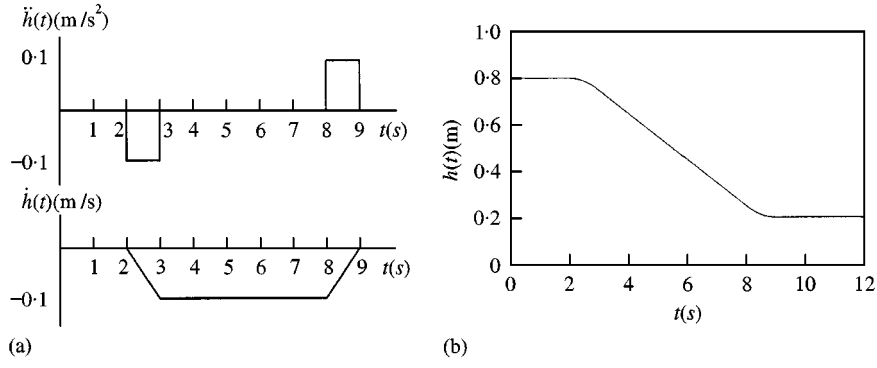

Figure 6. The acceleration, velocity and position profiles of the moving mass for the downward motion: (a) accleration and velocity profiles of the moving mass; (b) position profile of the moving mass.

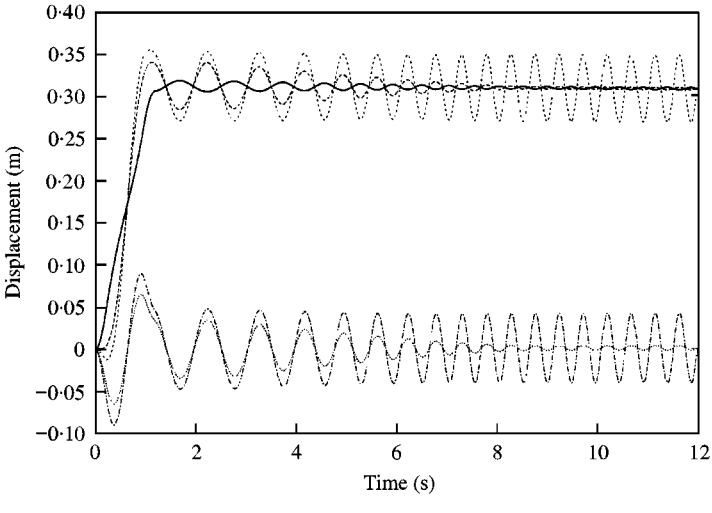

Figure 7. The open-loop responses of the beam-mass-cart system by the forcing function (35) and the trajectory of moving mass in Figure 6 when $m = 2$ kg: (—), $x(t)$; (– –), $x_h(t)$; (– – –), $x_T(t)$; (· · ·), w_h; (– · – ·), $w_T(t)$.

in XY plane with the mass. Since the purpose of this study is the investigation of the vibrational motion of the elastic beam, the desired path is planned without considering the flexibility of elastic beam. The force to be applied to the cart, $f_1(t)$, is generated as

$$f_1(t) = M_t[\ddot{\alpha}_d + K_v(\dot{\alpha}_d - \dot{\alpha}) + K_p(\alpha_d - \alpha)] \tag{37}$$

to follow the desired trajectory of the center of mass of the beam–mass–cart system as

$$\alpha_d(t) = x_c - R\sin(\Omega t), \tag{38}$$

because $\alpha(t) = x(t)$ in the case of rigid beam. Further, it is assumed that the force to be applied to the moving mass, $f_2(t)$, is made to generate the desired vertical trajectory of the moving mass to follow

$$h_d(t) = y_c \pm R\cos(\Omega t). \tag{39}$$

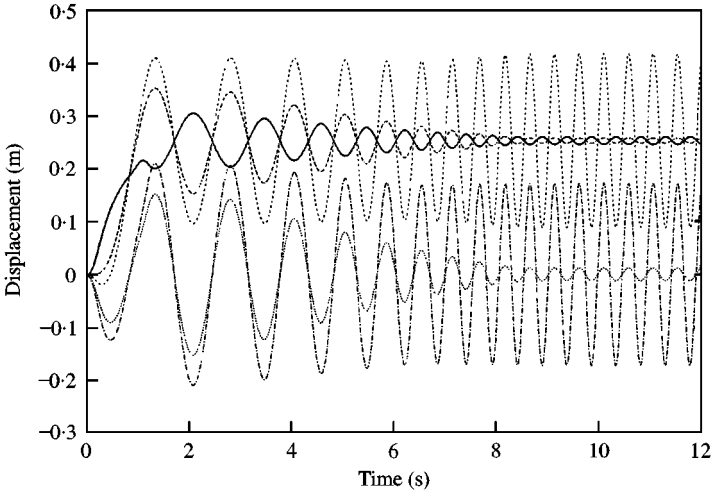

Figure 8. The open-loop responses of the beam-mass-cart system by the forcing function (35) and the trajectory of moving mass in Figure 6 when $m = 5$ kg: (—), $x(t)$; (– –), $x_h(t)$; (– – –), $x_T(t)$; (· · ·), w_h; (– · – ·), $w_T(t)$.

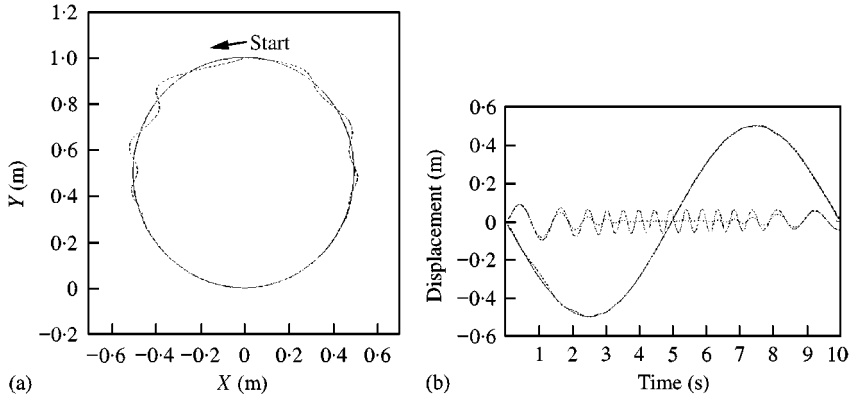

Figure 9. The trajectory of the moving mass and time response of the beam-mass-cart system when $m = 2$ kg and $\Omega = 2\pi/10$. In (a), (—), desired trajectory of moving mass; (– –) simulated trajectory of moving mass, in (b), (—), $\alpha_d(t)$; (– –), $x(t)$; (- - -), w_h; (· · ·), $w_T(t)$. (a) trajectory; (b) time response.

Figure 9 shows the simulated trajectory of the moving mass and the tip of the elastic beam with respect to the desired one in (a) and $x(t)$, w_h and $w_T(t)$ in (b) when $m = 2$ kg, $(x_c, y_c) = (0, 0{\cdot}5)(m)$, $R = 0{\cdot}5\ m$, $K_p = 15$, $K_v = 15$, $\Delta h = l/200$, $p = 3$, $\Omega = 2\pi/10$ and the system parameters given in Table 1 are used. The moving mass moves in counter-clockwise direction from the start point $(X, Y) = (0, 1)$.

Figure 10 shows the result under the same conditions with the previous simulation when $m = 5$ kg. Figure 11 shows the simulated result when the moving mass moves in clockwise direction from the start point $(X, Y) = (0, 0)$ and all the conditions are identical with those used in the previous simulations.

As seen in the results, the effect of the vibration of the beam–mass system to that of the base cart becomes greater as the moving mass becomes heavier. Furthermore, w_h becomes smaller as the moving mass goes down from the upper position to lower one while the

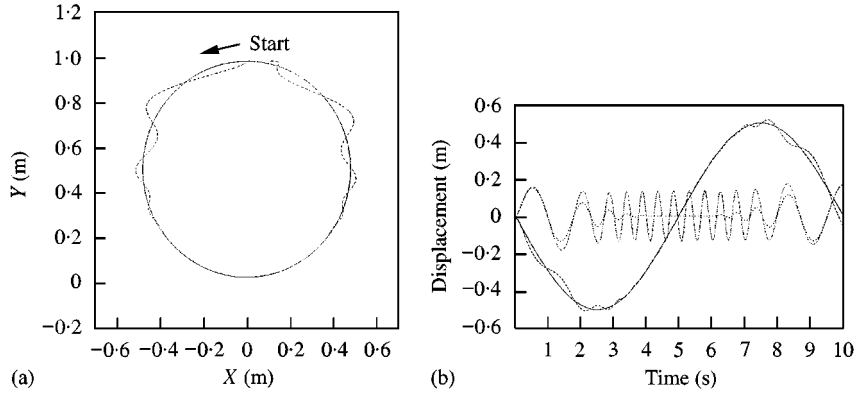

Figure 10. The trajectory of the moving mass and time response of the beam-mass-cart system when $m = 5$ kg and $\Omega = 2\pi/10$. In (a), (—), desired trajectory of moving mass; (– –), simulated trajectory of moving mass; in (b), (—), $\alpha_d(t)$; (– –), $x(t)$; (- - -), w_h; (···), $w_T(t)$. (a) trajectory; (b) time response.

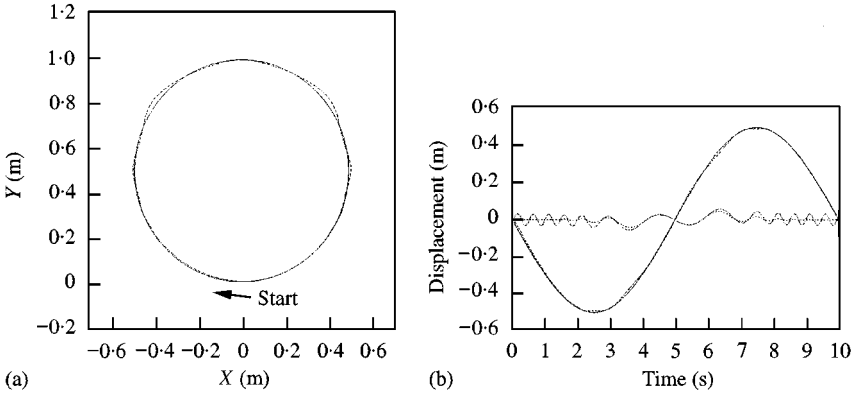

Figure 11. The trajectory of the moving mass and time response of the beam-mass-cart system when $m = 5$ kg and $\Omega = 2\pi/10$. In (a), (—), desired trajectory of moving mass; (– –), simulated trajectory of moving mass; in (b), (—), $\alpha_d(t)$, (– –), $x(t)$; (- - -), w_h; (···), $w_T(t)$. (a) trajectory; (b) time response.

vibration becomes fast. On the contrary, when the moving mass goes up, w_h becomes larger while the vibration becomes slow. The results show the physical phenomena well. Comparing the result in Figures 10 and 11, vibration of the beam–mass–cart system becomes smaller when the moving mass starts at low position than it starts at high position.

It is natural, in numerical calculation, that the simulated results describe the real plant closer as the step size of the change of the position of the moving mass, Δh, and the size of time step for numerical integration, Δt, become finer, and as more number of modes for expanding the deflection, p in equation (33), is considered. In these simulations, the size of time step for numerical integration was chosen as $\Delta t = 2\pi/100\omega_p$, where ω_p is the natural frequency of pth mode. This scheme can guarantee the accuracy of numerical integration though the natural frequencies of the beam–mass–cart system vary along the position of the moving mass.

The step size of the change of the position of the moving mass, Δh, was chosen as $l/200$. The difference of w_h at steady state in Figure 5 between $\Delta h = l/200$ and $l/500$ is under 8%.

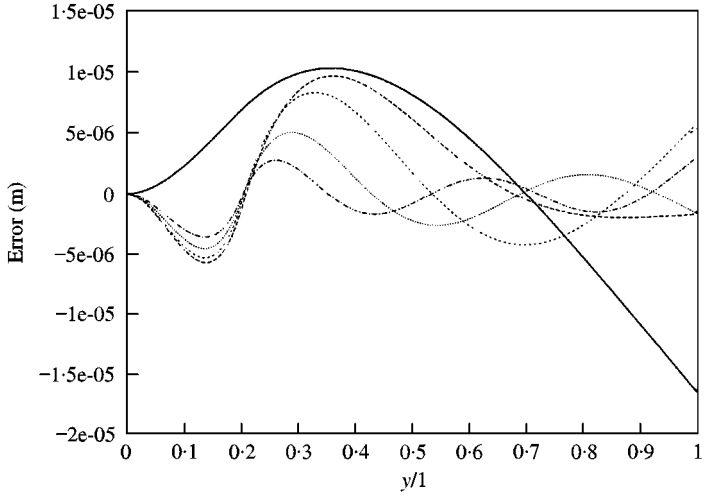

Figure 12. The error between the two expansions of deflection in equation (33) for the first change of the step of the position of the moving mass when $\Delta h = l/200$ (in the simulation for Figure 3): (—), $p = 1$; (– –), $p = 2$; (- - -), $p = 3$; (···), $p = 4$; (–·–·), $p = 5$.

However, as Δh becomes finer w_h at steady state is bounded in this error range. For example, the difference of w_h at steady state in Figure 5 between $\Delta h = l/200$ and $l/1000$ is 4·5% and those between $\Delta h = l/200$ and $l/5000$ is 2·3%.

The number of modes, p, in expanding the deflection of the beam and the position of the cart as in equations (33) and (34), respectively, also effects the accuracy of the result. The number of modes, p, considered for the simulations in this paper is 3. The difference of the simulated responses with the number of modes over 3 is negligible in mechanical sense. As an example, the simulation for Figure 3 was considered and Figure 12 shows the error between the two expansions of deflection in equation (33) for the first change of the step of the position of the moving mass when $\Delta h = l/200$. As seen in the figure, the error is sufficiently small with $p = 3$.

The analytical method introduced in this paper gives satisfactory results in a mechanical sense with minimum number of modes in expanding the deflection of the elastic beam because the exact normal mode solutions corresponding to the eigenfrequencies of the beam–mass–cart system with respect to the position of the moving mass and the weight ratio of the system are used.

5. EXPERIMENTAL VERIFICATION

5.1. EXPERIMENTAL SET-UP

Figure 13 shows the experimental set-up. As seen in Figure 13(a) and 13(b), a thin flexible beam carrying a concentrated or a moving mass is clamped on the moving carriage of a linear motor by a beam fixture. The linear motor used as the moving base is LEB-S-2-S made by ANORAD Co. Figure 13(c) shows the moving mass. The moving mass moves along the flexible beam by two pairs of rubber-coated wheels driven by an AC servo motor and a reduction gear. Table 2 shows the specification of the experimental set-up.

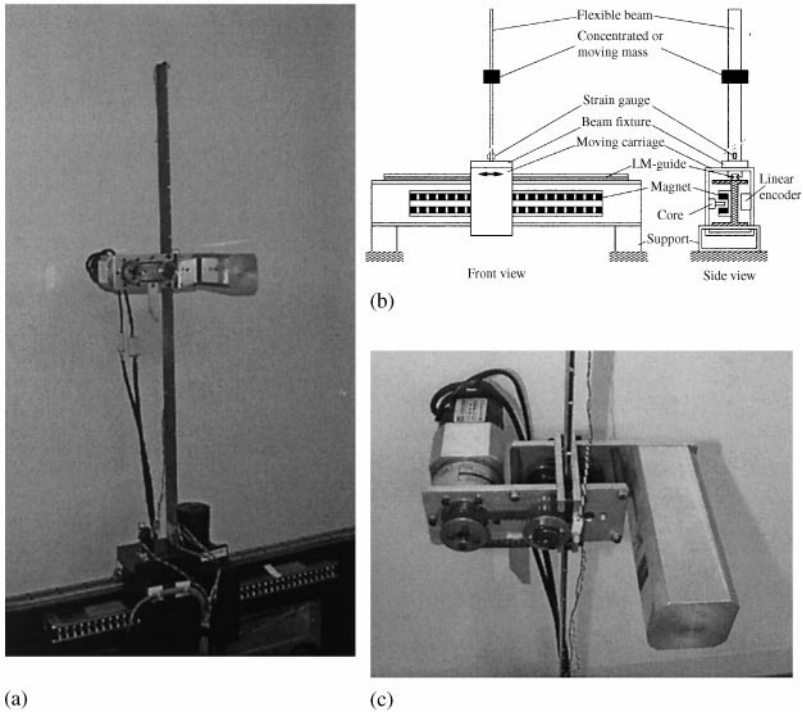

Figure 13. The experimental set-up: (a) photograph of the experimental set-up; (b) Schematics of the experimental setup; (c) photograph of the moving mass.

TABLE 2

Specifications of the experimental set-up

Moving base	
Continuous force of linear motor	103 N
Maximum moving velocity	2·0 m/s
Maximum moving distance	0·5 m
Resolution of linear encoder	2 μm
Mass of the moving carriage	5·04 kg
Mass of the beam fixture	4·61 kg
Beam 1	
Dimension ($L \times W \times T$)	$1000 \times 50 \times 3{\cdot}12$ mm
Mass per unit length, ρ_0	1·2168 kg/m
Area moment of inertia, I	$1{\cdot}265 \times 10^{-10}$ m^4
Young's modulus, E	$2{\cdot}07 \times 10^{11}$ N/m
Beam 2	
Dimension ($L \times W \times T$)	$1000 \times 49{\cdot}85 \times 3{\cdot}8$ mm
Mass per unit length, ρ_0	1·4776 kg/m
Area moment of inertia, I	$2{\cdot}279 \times 10^{-10}$ m^4
Young's modulus, E	$2{\cdot}07 \times 10^{11}$ N/m
Moving mass	
Rated power of AC servo motor	100 W
Rated torque of AC servo motor	0·32 Nm
Rated speed of AC servo motor	3000 rev/min
Gear reduction rate	10:1
Total weight	5·4 kg

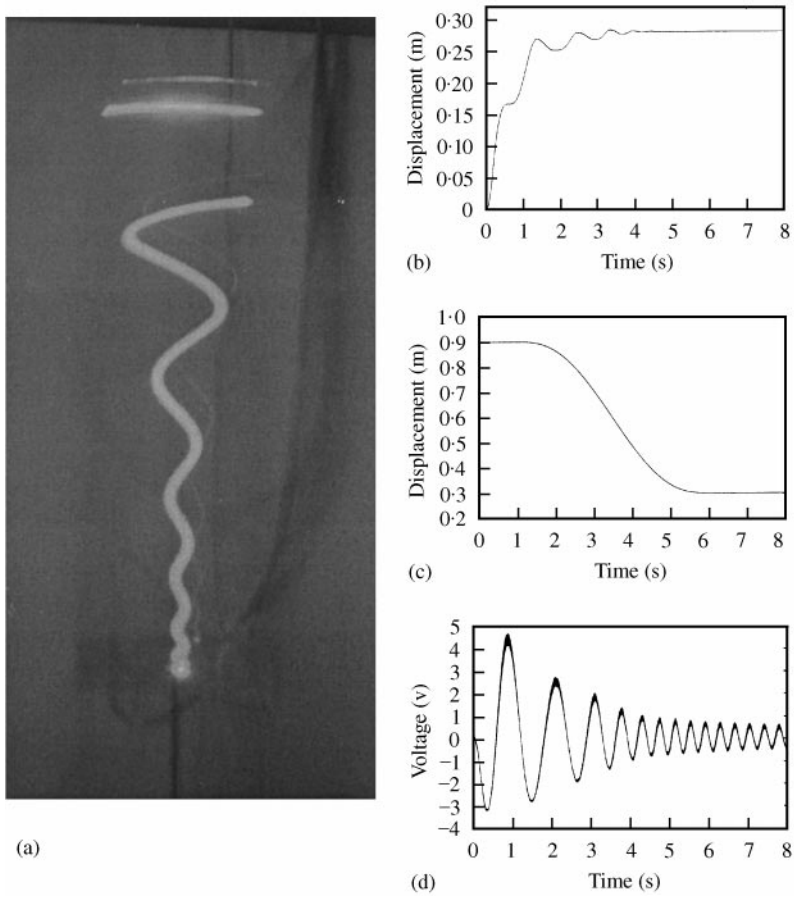

Figure 14. Open-loop responses for the linear motion of the moving mass (up-to-down motion): (a) trajectory of the moving mass in XY plane (up-to-down); (b) cart position; (c) vertical trajectory of the moving mass; (d) strain signal.

5.2. LINEAR MOTION OF THE MOVING MASS

The open-loop responses of the beam–mass–cart system with a linearly moving mass are verified by experiments. For these experiments, the base cart on which the beam 1 in Table 2 carrying the moving mass is mounted is excited by the driving force

$$f_1(t) = \begin{cases} 30N & \text{when } 0 < t \leqslant 0{\cdot}2 \text{ s}, \\ 0N & \text{when } t > 0{\cdot}2 \text{ s}. \end{cases} \tag{40}$$

The moving mass was controlled by the robust internal-loop compensator (RIC) [22] to robustly follow the given trajectories even under the disturbances such as friction and the dynamics due to the vibration of the beam.

Figure 14 shows the open-loop response of the beam–mass–cart system when the moving mass follows the trajectory in figure 14(c) along the flexible beam. Figure 14(a) is the global trajectory of the moving mass in XY plane. The trajectory was obtained by taking the picture of an LED attached to the moving mass after the moving base is translated by the applied force. The upper semi-arc line is caused by the other LED attached to the top end of

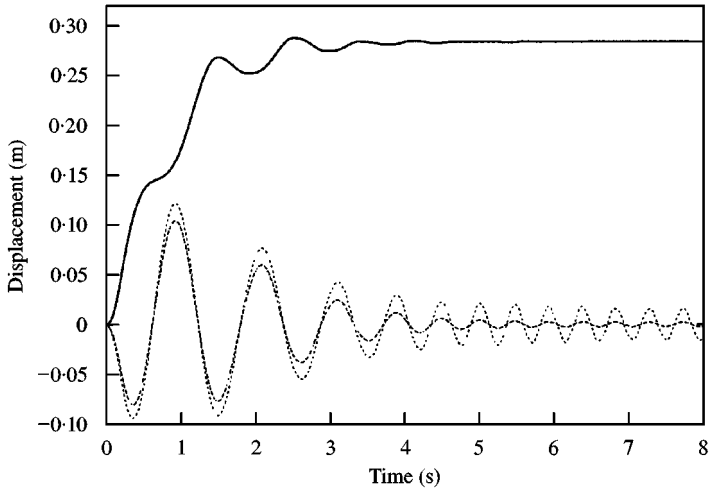

Figure 15. Simulation results for the linear motion of the moving mass (up-to-down): (—) $x(t)$; (– –), w_h; (- - -), $w_T(t)$.

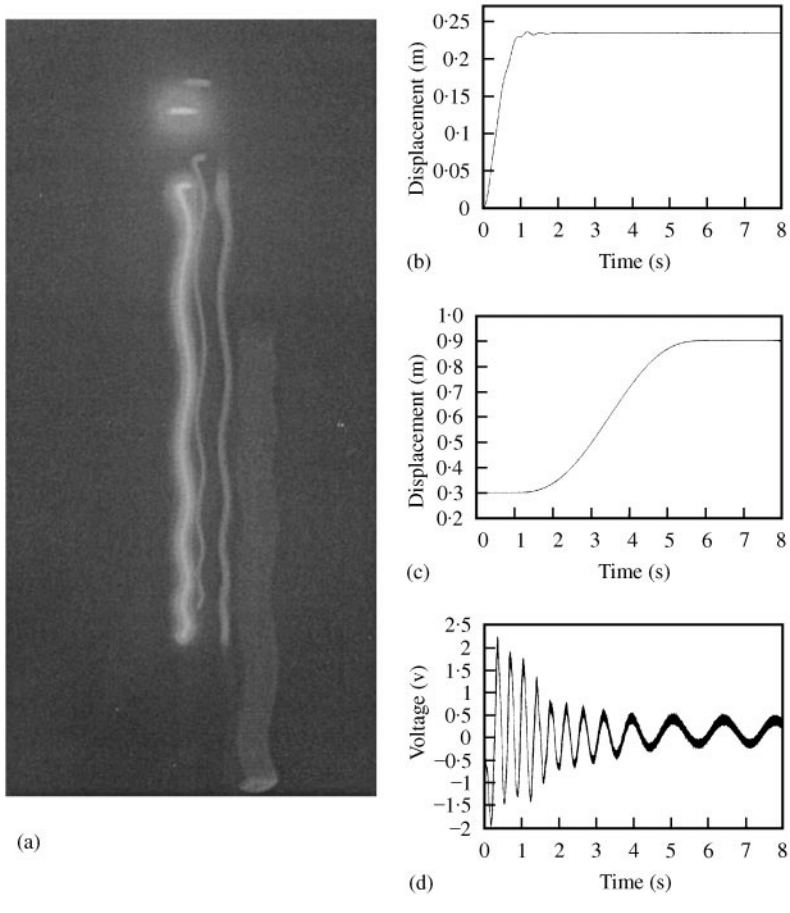

Figure 16. Open-loop responses for the linear motion of the moving mass (up-to-down motion): (a) trajectory of the moving mass in XY plane (down-to-up); (b) cart position; (c) vertical trajectory of the moving mass; (d) strain signal.

the beam. Figure 14(b) is the position of the cart measured by the linear encoder of the linear motor. As seen in Figure 14(b), the cart stops at a position without the deceleration command due to the friction between the moving carriage and the LM-guide of the linear motor. Figure 14(c) is the time trajectory of the moving mass measured by the encoder of the servo motor of the moving mass. The maximum error between the reference trajectory and the measured one in this experiment is less than 0·7 mm in spite of the large friction between the flexible beam and the moving mass. Figure 14(d) is the strain signal measured by strain guages attached to the root of the flexible beam.

Figure 15 shows the simulation results for the same conditions with the previous experiment. In this simulation the friction force between the moving carriage and the LM-guide of the linear motor is modelled as

$$F_{fric} = \begin{cases} 0 & \text{when } \dot{x} = 0, \\ f_{st} \cdot \operatorname{sgn}(\dot{x}) & \text{when } 0 \leqslant |\dot{x}| \leqslant \varepsilon, \\ f_c \cdot \operatorname{sgn}(\dot{x}) + f_v \dot{x} & \text{when } |\dot{x}| > \varepsilon, \end{cases} \tag{41}$$

where f_{st} and f_c are the static and the Coulomb friction forces, and f_v is the viscous friction coefficient, respectively, and ε is a positive infinitesimal value. The friction coefficients used in these simulation are $f_{st} = 5{\cdot}0$, $f_c = 3{\cdot}5$, and $f_v = 2{\cdot}35$. Considering that the friction coefficients have some error and that the natural frequencies of the system differ a little from those by equations (28) and (24) due to the friction force [12], the simulation results match remarkably well with that of experiments, especially for the cart positions and the tip deflections.

Figure 16 shows the open-loop response of the beam–mass–cart system when the moving mass follows the trajectory in Figure 16(c) along the flexible beam. Figure 16(a) is the global trajectory of the moving mass in XY plane. Figure 16(b) is the position of the cart measured by the linear encoder of the linear motor Figure 16(c) is the time trajectory of the moving mass measured by the encoder of the servo motor of the moving mass. The maximum error between the reference trajectory and the measured one in this experiment is less than 0·5 mm. (d) is the strain signal measured by strain gauges attached to the root of the flexible beam.

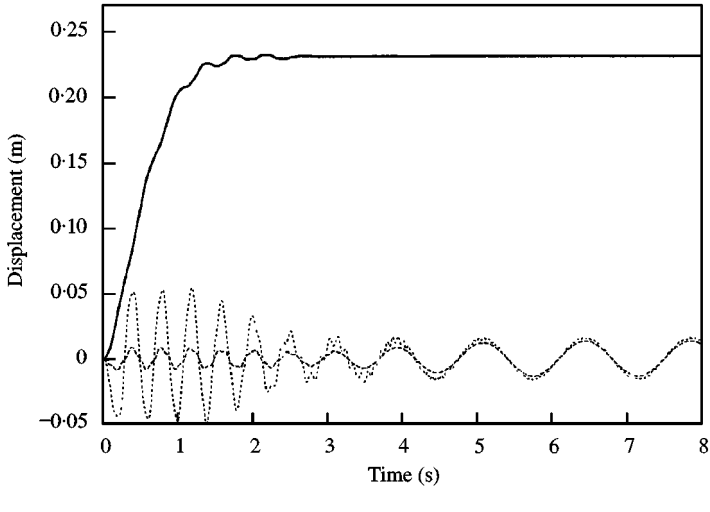

Figure 17. Simulation results for the linear motion of the moving mass (down-to-up): (—) $x(t)$; (– –), $w_h(t)$; (– – –), $w_T(t)$.

Figure 17 shows the simulation results for the same conditions with the previous experiment. Under the consideration that there are some errors in the friction coefficients, and that the beam has damping effects not considered in the simulation, the simulation results show well the dynamic behavior obtained from the experiment.

5.3. CIRCULAR MOTION OF THE MOVING MASS

The responses of the beam–mass–cart system for the circular motion of the moving mass in XY plane are verified by experiments. For these experiments, the base cart on which the beam

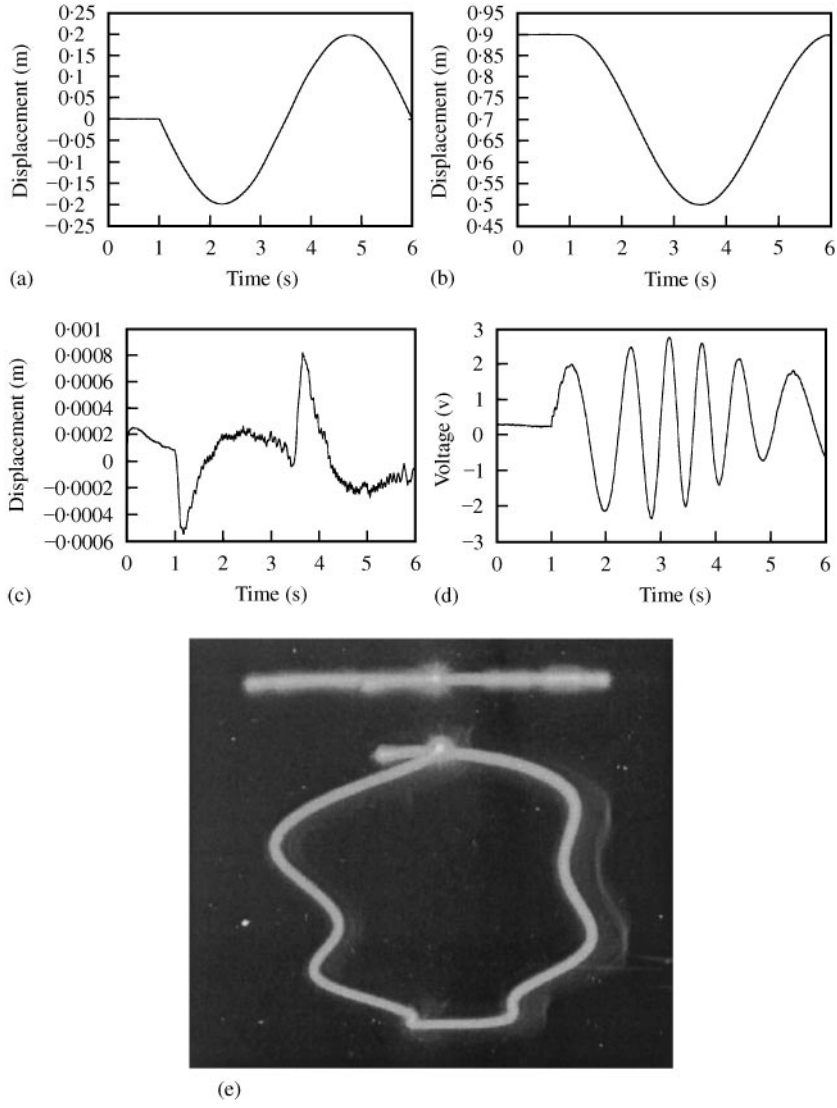

Figure 18. Experimental results for the circular motion of the moving mass when $R = 0{\cdot}2$, $\Omega = 2\pi/5$, $K_p = 250$, and $K_v = 7{\cdot}5$: (a) position of the base cart, $x(t)$; (b) position of the moving mass, $h(t)$; (c) the error between $h_d(t)$ and $h(t)$; (d) strain signal; (e) the trajectory of the moving mass in XY plane.

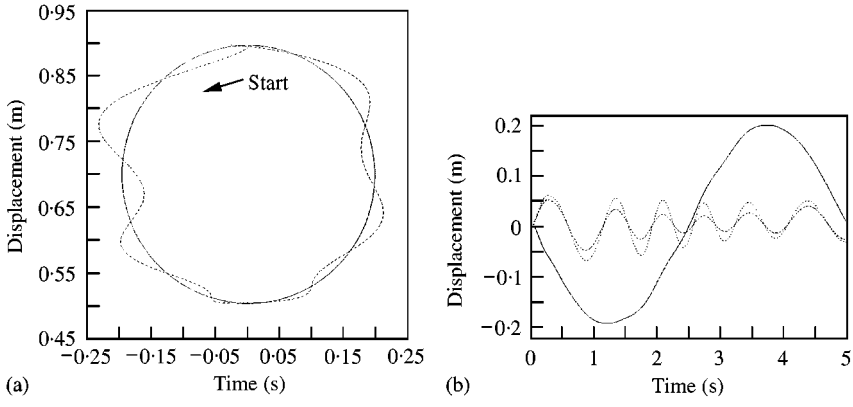

Figure 19. The trajectory of the moving mass and time response of the beam-mass-cart system when $\Omega = 2\pi/5$, $K_p = 250$ and $K_v = 7{\cdot}5$. In (a), (—), desired trajectory of moving mass; (– –), simulated trajectory of moving mass; in (b), (—), $x(t)$; (– –), w_h; (- - -), $w_T(t)$: (a) trajectory; (b) time response.

2 in Table 2 carrying the moving mass is mounted is controlled by the controller

$$f_1(t) = M_t[\ddot{x}_d + K_v(\dot{x}_d - \dot{x}) + K_p(x_d - x)]. \tag{42}$$

The desired trajectory of the base cart is designed as

$$x_d(t) = x_c - R\sin\Omega t, \tag{43}$$

and it is assumed that the RIC makes the moving mass to follow the trajectory

$$h_d(t) = y_c + R\cos\Omega t. \tag{44}$$

Figure 18 shows the experimental results when the moving mass follows the circular path given by equations (43) and (44) with radius $R = 0{\cdot}2$ and $\Omega = 2\pi/5$. The moving mass starts from $(x_c, y_c) = (0{\cdot}0, 0{\cdot}9)$ to CCW direction after 1*s*, and the feedback gains K_p and K_v are 250 and 7·5 respectively. Figure 18(a) is the time response of the moving base, $x(t)$, measured by the linear encoder of the linear motor. Figure 18(b) is the time response of the moving mass, $h(t)$. Figure 18(c) is the position error between $h_d(t)$ and $h(t)$. The position error is sufficiently small due to the RIC. Figure 18(d) is the strain signal measured by the strain gauges attached to the root of the elastic beam. Figure 18(e) is the global trajectory of the moving mass obtained by taking picture of a LED attached to the moving mass.

Figure 19 is the simulation results using the analytical method developed in this study for the same conditions with the previous experiment. It is difficult to compare the experimental results with that of simulation quantitatively because it is difficult to measure the global position of the moving mass. However, it can be known that the simulation results by the proposed analytical method describes the experimental results very well except for some difference in natural frequencies of the system.

Figure 20 shows the experimental results when the same conditions with the previous experiment are used except that $K_p = 140{\cdot}6$ and $K_v = 5{\cdot}6$. Smaller feedback gains produce less distorted trajectory of the moving mass than the previous one. Figure 21 is the simulation results for the same conditions with the previous experiment. The simulation results match well with the experimental ones.

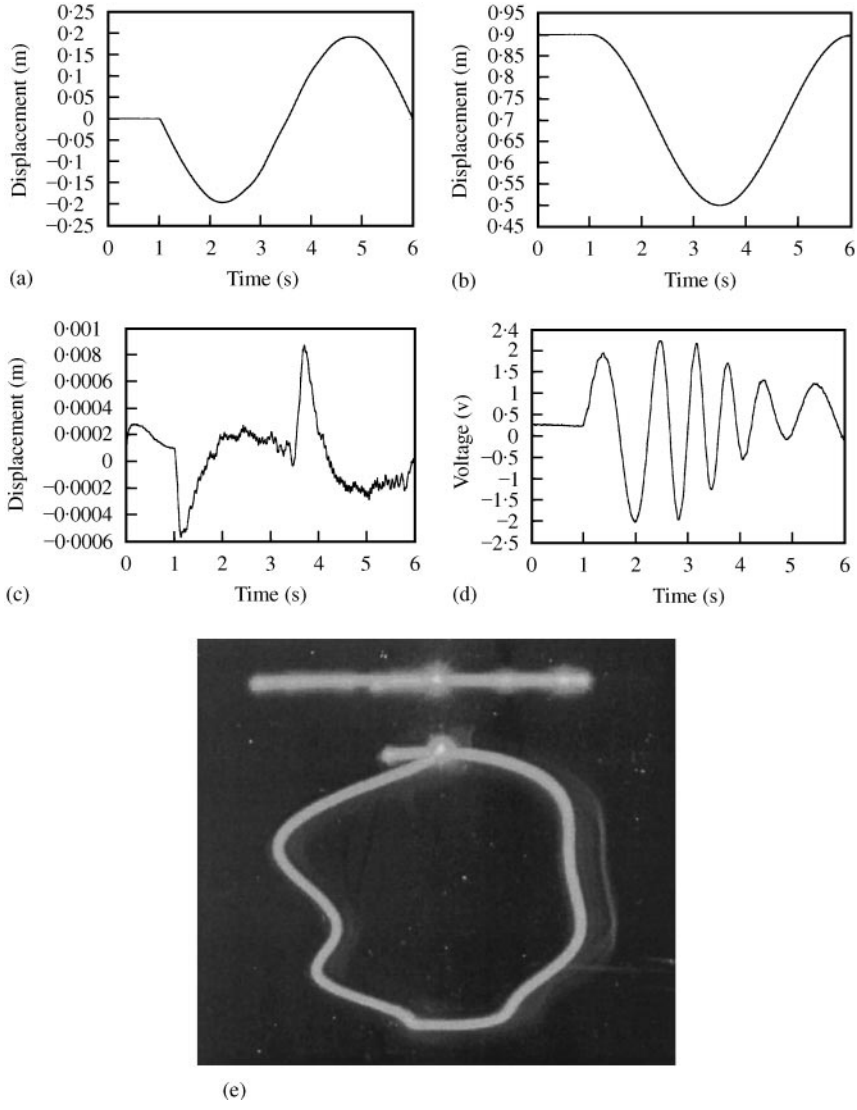

Figure 20. Experimental results for the circular motion of the moving mass when $R = 0{\cdot}2$, $\Omega = 2\pi/5$, $K_p = 140{\cdot}6$, and $K_v = 5{\cdot}6$; (a) position of the base cart; (b) position of the moving mass; (c) the error between $h_d(t)$ and $h(t)$; (d) strain signal; (e) the trajectory of the moving mass in XY plane.

6. CONCLUDING REMARKS

In this study, the equation of motion of an elastic beam fixed on a moving cart and carrying a moving mass was derived and the coupled dynamic equations were solved by unconstrained modal analysis. An analytical method utilizing the exact normal mode solutions corresponding to the eigenfrequencies for the position of the moving mass and the ratios of the weight of the beam–mass–cart system was proposed. The proper transformation of the time solutions between the normal modes for a position and those for the next position of the moving mass were also adopted in the analysis.

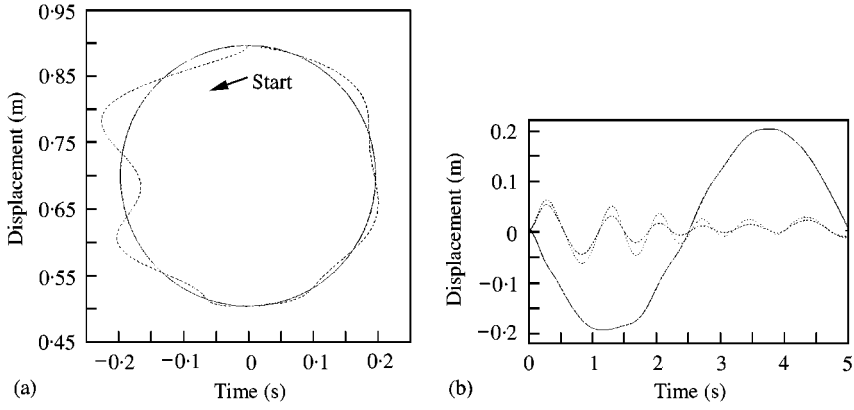

Figure 21. The trajectory of the moving mass and time response of the beam-mass-cart system when $\Omega = 2\pi/5$, $K_p = 140{\cdot}6$, and $K_v = 5{\cdot}6$; (a), (—), desired trajectory of moving mass; (– –), simulated trajectory of moving mass; in (b), (—), $x(t)$; (– –), w_h; (- - -), $w_T(t)$; (a) trajectory; (b) time response.

Numerical simulations were carried out to verify the validity of the proposed method, and the open-loop responses of the system in tracking the pre-designed path of the moving mass were obtained. The simulation results show the dynamic behavior of the beam–mass–cart system well and this method can be used as a motion simulator which describes the vibrational motion of a moving elastic beam with a moving mass. Those analytical results were compared with the experimental ones. The experimental results show the validity of the analytical method proposed in this study.

For further study, active vibration suppression controller using the dynamics of the system would be designed.

ACKNOWLEDGMENT

The authors would like to thank Dr. Kitae Lee in the Department of Physics in POSTECH for his helpful comments on developing the numerical codes used in this study. We thank Mr. Bong Keun Kim, a Ph.D. student in our laboratory, for his kind help in carrying out the experiments using the RIC. Thanks also belong to the referees who reviewed this article and gave good comments to enhance the quality of this paper.

REFERENCES

1. R. S. AYRE, L. S. JACOBSEN and C. S. HSU 1951 *Proceedings of the First U.S. National Congress of Applied Mechanics*, 81–90. Transverse vibration of one- and of two-span beams under the action of a moving mass load.
2. J. T. KENNEY, JR 1954 *American Society of Mechanical Engineers, Journal of Applied Mechanics* **21**, 359–364. Steady-state vibrations of beam on elastic foundation for moving load.
3. C. R. STEELE 1967 *American Society of Mechanical Engineers, Journal of Applied Mechanics* **34**, 111–118. The finite beam with a moving mass.
4. H. D. NELSON and R. A. CONOVER 1971 *American Society of Mechanical Engineers, Journal of Applied Mechanics* **93**, 1003–1006. Dynamic stability of a beam carrying moving masses.
5. M. M. STANIŠIĆ and J. C. HARDIN 1969 *Journal of Franklin Institute* **287**, 115–123. On the response of beams to an arbitrary number of concentrated moving mass.
6. E. C. TING, J. GENIN and J. H. GINSBERG 1974 *Journal of Sound and Vibration* **33**, 49–58. A general algorithm for moving mass problems.

7. M. OLSSON 1991 *Journal of Sound and Vibration* **145**, 299–307. On the fundamental moving load problem.
8. S. MACKERTICH 1992 *Journal of Acoustical Society of America* **92**, 1766–1769. Response of a beam to a moving mass.
9. H. P. LEE 1996 *Journal of Sound and Vibration* **191**, 289–294. Dynamic responses of a beam with a moving mass.
10. U. LEE 1998 *Journal of Sound and Vibration* **209**, 867–877. Separation between the flexible structure and the moving mass sliding on it.
11. M. A. FODA and Z. ABDULJABBER 1998 *Journal of Sound and Vibration* **210**, 295–306. A dynamic Green formulation for the response of a beam structure to a moving mass.
12. S. PARK, W. K. CHUNG, Y. YOUM and J. W. LEE 2000 *Journal of Sound and Vibration* **230**, 591–615. Natural frequencies and open-loop responses of an elastic beam fixed on a moving cart and carrying an intermediate lumped mass.
13. L. MEIROVITCH 1980 *Computational Methods in Structural Dynamics*, MD: Si-Jthoff & Noordhoff.
14. L. MEIROVITCH 1993 *Shock and Vibration* **1**, 107–119. Derivation of equations for flexible multibody systems in terms of quasi-coordination from the extended Hamilton's principle.
15. U. LEE, C. H. PARK and S. C. HONG 1995 *Journal of Sound and Vibration* **180**, 297–311. The dynamics of a piping system with internal unsteady flow.
16. S. SADIKU and H. H. E. LEIPHOLZ 1987 *Ingenieur-Archiv* **57**, 223–242. On the dynamics of elastic system with moving concentrated masses.
17. E. BARBIERI and Ü. ÖZGÜNER 1988 *Transaction of Dynamic System Measurement and Control* **110**, 416–421. Unconstrained and constrained mode expansion for a flexible slewing link.
18. C. C. DE WIT, B. SICILIANO and G. BASTIN 1996 *Theory of Robot Control*. Berlin: Springer.
19. M. M. STANIŠIĆ and S. T. MONTGOMERY 1974 *Ingenieur–Archiv* **43**, 295–305. On a theory concerning the dynamical behavior of structures carrying moving masses.
20. R.-F. FUNG, P.-Y. LU and C.-C. TSENG *Journal of Sound and Vibration* **218**, 559–571. Non-linearly dynamic modeling of an axially moving beam with a tip mass.
21. H. YAMAZAKI, T. ONO and C. Y. PARK 1996 *Proceedings of the 11th Korea Automatic Control Conference* (*KACC*), 405–408. Trajectory control of the flexible manipulator with time-varying arm.
22. B. K. KIM, H. T. CHOI, W. K. CHUNG and Y. H. CHANG 1999 *Proceedings of IEEE International Symposium on Industrial Electronics*, 1045–1050. Robust optimal internal loop compensator design for motion control of precision linear motor.

APPENDIX A

Substituting equation (8), variations of equations (9)–(11) into equation (7), one obtains

$$\int_{t_1}^{t_2}\left\{\frac{\partial L_r}{\partial \dot{x}}\delta\dot{x}+\int_0^l\left(\frac{\partial L_e}{\partial \dot{x}}\delta\dot{x}+\frac{\partial L_e}{\partial \dot{w}}\delta\dot{w}+\frac{\partial L_e}{\partial w'}\delta w'+\frac{\partial L_e}{\partial w''}\delta w''+\frac{\partial L_e}{\partial \dot{h}}\dot{h}+\frac{\partial L_e}{\partial h}\delta h\right)\mathrm{d}y\right.$$
$$\left.+f_1(t)\delta x+\frac{f_2(t)}{\cos\theta}\delta h\right\}\mathrm{d}t=0. \tag{A.1}$$

Integrating equation (A.1) by parts and considering that t_1 and t_2 are arbitrary, the following equations are obtained:

$$\frac{\mathrm{d}}{\mathrm{d}t}\left(\frac{\partial L_r}{\partial \dot{x}}\right)+\int_0^l\frac{\mathrm{d}}{\mathrm{d}t}\left(\frac{\partial L_e}{\partial \dot{x}}\right)\mathrm{d}y-f_1(t)=0, \tag{A.2}$$

$$\int_0^l\left[\frac{\mathrm{d}}{\mathrm{d}t}\left(\frac{\partial L_e}{\partial \dot{w}}\right)+\frac{\partial}{\partial y}\left(\frac{\partial L_e}{\partial w'}\right)-\frac{\partial^2}{\partial y^2}\left(\frac{\partial L_e}{\partial w''}\right)\right]\delta w\,\mathrm{d}y=0, \tag{A.3}$$

$$\int_0^l\left[\frac{\mathrm{d}}{\mathrm{d}t}\left(\frac{\partial L_e}{\partial \dot{h}}\right)-\frac{\partial L_e}{\partial h}-\delta(y-h)\frac{f_2(t)}{\cos\theta}\right]\delta h\,\mathrm{d}y=0, \tag{A.4}$$

$$\frac{\partial L_e}{\partial w''}\,\delta w'\Big|_{y=0}^{y=l} = 0, \tag{A.5}$$

$$-\frac{\partial L_e}{\partial w'}\,\delta w\Big|_{y=0}^{y=1} + \frac{\partial}{\partial y}\left(\frac{\partial L_e}{\partial w''}\right)\delta w\Big|_{y=0}^{y=1} = 0. \tag{A.6}$$

Substitution of equations (9) and (10) into equations (A.2)–(A.6) gives the equations of motion and the boundary conditions in equations (12)–(15). In deriving equation (12), the second term on the left-hand side of equation (A.2) is obtained as

$$\begin{aligned}\int_0^l \frac{\mathrm{d}}{\mathrm{d}t}\left(\frac{\partial L_e}{\partial \dot{x}}\right)\mathrm{d}y &= \int_0^l \frac{\mathrm{d}}{\mathrm{d}t}\{[\rho_0 + m\delta(y-h)](\dot{x}+\dot{w}) + m\delta(y-h)\dot{h}w'\}\,\mathrm{d}y\\ &= \int_0^l \{[\rho_0 + m\delta(y-h)](\ddot{x}+\ddot{w}) + m\delta(y-h)(\ddot{h}w' + \dot{h}\dot{w}')\\ &\qquad - m\dot{h}\delta'(y-h)(\dot{x}+\dot{w}+\dot{h}w')\}\,\mathrm{d}y \qquad \text{(A.7)}\\ &= \int_0^l \{[\rho_0 + m\delta(y-h)](\ddot{x}+\ddot{w}) + m\delta(y-h)[\ddot{h}w' + 2\dot{h}\dot{w}' + \dot{h}^2 w'']\}\,\mathrm{d}y,\end{aligned}$$

where the relations

$$\frac{\mathrm{d}}{\mathrm{d}t}\,\delta(y-h) = \frac{\mathrm{d}h}{\mathrm{d}t}\frac{\mathrm{d}}{\mathrm{d}h}\,\delta(y-h) = -\dot{h}\delta(y-h) \tag{A.8}$$

and

$$\int_0^l \delta'(y-h)f(y)\,\mathrm{d}y = -\int_0^l \delta(y-h)f'(y)\,\mathrm{d}y \tag{A.9}$$

are used.

In deriving equation (13), one obtains the first term on the left-hand side in equation (A.3) as

$$\begin{aligned}&\int_0^l \frac{\mathrm{d}}{\mathrm{d}t}\left(\frac{\partial L_e}{\partial \dot{w}}\right)\mathrm{d}y\\ &= \int_0^l \frac{\mathrm{d}}{\mathrm{d}t}\{[\rho_0 + m\delta(y-h)](\dot{x}+\dot{\omega}) + m\delta(y-h)\dot{h}w'\}\,\delta w\,\mathrm{d}y \qquad \text{(A.10)}\\ &= \int_0^l \{[\rho_0 + m\delta(y-h)](\ddot{x}+\ddot{w}) + m\delta(y-h)(\ddot{h}w' + \dot{h}\dot{w}')\\ &\qquad - m\dot{h}\delta'(y-h)(\dot{x}+\dot{w}+\dot{h}w')\}\,\delta w\,\mathrm{d}y,\end{aligned}$$

and for the second term as

$$\begin{aligned}\int_0^l \frac{\partial}{\partial y}\left(\frac{\partial L_e}{\partial w'}\right)\delta w\,\mathrm{d}y &= \int_0^l \frac{\partial}{\partial y}\{m\delta(y-h)[\dot{h}^2 w' + \dot{h}(\dot{x}+\dot{w})]\}\,\delta w\,\mathrm{d}y\\ &= \int_0^l \{m\delta(y-h)(\dot{h}^2 w'' + \dot{h}\dot{w}') + m\delta'(y-h)[\dot{h}^2 w' + \dot{h}(\dot{x}+\dot{w})]\}\,\delta w\,\mathrm{d}y.\end{aligned} \tag{A.11}$$

To derive the third equations of motion, equation (14), the first term on the right-hand side in equation (A.4) becomes

$$\begin{aligned}\int_0^l \frac{\mathrm{d}}{\mathrm{d}t}\left(\frac{\partial L_e}{\partial \dot{h}}\right)\delta h\,\mathrm{d}y &= \int_0^l \frac{\mathrm{d}}{\mathrm{d}t}\{m\delta(y-h)[\dot{h}(1+(w')^2)+w'(\dot{x}+\dot{w})]\}\,\delta h\,\mathrm{d}y\\ &= \int_0^l \{m\delta(y-h)[\ddot{h}(1+(w')^2)+2\dot{h}w'+\dot{w}'(\dot{x}+\dot{w})+w'(\ddot{x}+\ddot{w})]\\ &\quad - m\dot{h}\delta'(y-h)[\dot{h}(1+(w')^2))+w'(\dot{x}+\dot{w})]\}\,\delta h\,\mathrm{d}y \qquad (A.12)\\ &= \int_0^l m\delta(y-h)\{\ddot{h}[1+(w')^2]+2\dot{h}w'\dot{w}'+\dot{w}'(\dot{x}+\dot{w})+w'(\ddot{x}+\ddot{w})\\ &\quad + \dot{h}[2\dot{h}w'w''+w''(\dot{x}+\dot{w})+w'\dot{w}']\}\,\delta h\,\mathrm{d}y,\end{aligned}$$

and the second term becomes

$$\begin{aligned}&\int_0^l \frac{\partial L_e}{\partial \dot{h}}\,\delta h\,\mathrm{d}y\\ &= \int_0^l \left\{ -\tfrac{1}{2}m\delta'(y-h)(\dot{x}+\dot{w})^2 - \tfrac{1}{2}m\delta'(y-h)[\dot{h}^2(1+(w')^2)+2\dot{h}w'(\dot{x}+\dot{w})]\right.\\ &\quad \left. + m\delta'(y-h)gh - m\delta(y-h)g\right\}\delta h\,\mathrm{d}y \qquad (A.13)\\ &= \int_0^l m\delta(y-h)[\dot{x}\dot{w}'+\dot{w}\dot{w}'+\dot{h}^2w'w''+\dot{h}w''(\dot{x}+\dot{w})+\dot{h}w'\dot{w}'-g]\,\delta h\,\mathrm{d}y.\end{aligned}$$

APPENDIX B

In equation (22),

$$\begin{aligned}A_i(y) = \frac{m\omega^2}{4EIk_i^3}\Bigg\{&\frac{\mathrm{c}k_iy-\mathrm{ch}k_iy}{1+\mathrm{c}k_il\mathrm{ch}k_il}[(\mathrm{s}k_i(l-\bar{h})+\mathrm{sh}k_i(l-\bar{h}))(\mathrm{c}k_il+Chk_il)\\ &-(\mathrm{c}k_i(l-\bar{h})+\mathrm{ch}k_i(l-\bar{h}))(\mathrm{s}k_il+\mathrm{sh}k_il)]\\ &+\frac{\mathrm{s}k_iy-\mathrm{sh}k_iy}{1+\mathrm{c}k_il\mathrm{ch}k_il}[(\mathrm{s}k_i(l-\bar{h})+\mathrm{sh}k_i(l-\bar{h}))(\mathrm{s}k_il-\mathrm{sh}k_il) \qquad (B.1)\\ &+(\mathrm{c}k_i(l-\bar{h})+\mathrm{ch}k_i(l-\bar{h}))(\mathrm{c}k_il+\mathrm{ch}k_il)]\\ &-2U(y-\bar{h})[\mathrm{s}k_i(y-\bar{h})-\mathrm{sh}k_i(y-\bar{h})]\Bigg\},\end{aligned}$$

$$\begin{aligned}B_i(y) = \tfrac{1}{2}\Bigg[&\mathrm{c}k_iy+\mathrm{ch}k_iy-\frac{\mathrm{s}k_il\mathrm{sh}k_il}{1+ck_il\mathrm{ch}k_il}(\mathrm{c}k_iy-\mathrm{ch}k_iy)\\ &+\frac{\mathrm{c}k_il\mathrm{sh}k_il+\mathrm{s}k_il\mathrm{ch}k_il}{1+\mathrm{c}k_il\mathrm{ch}k_il}(\mathrm{s}k_iy-\mathrm{sh}k_iy)\Bigg], \qquad (B.2)\end{aligned}$$

$$C_i = -\frac{m}{2M}\frac{1}{1+\mathrm{c}k_i l\mathrm{ch}k_i l}\{[\mathrm{c}k_i(l-\bar{h})+\mathrm{ch}k_i(l-\bar{h})](\mathrm{c}k_i l+\mathrm{ch}k_i l) + [\mathrm{s}k_i(l-\bar{h})+\mathrm{sh}k_i(l-\bar{h})](\mathrm{s}k_i l-\mathrm{sh}k_i l)\}, \tag{B.3}$$

$$D_i = -\frac{\rho_0}{Mk_i}\frac{\mathrm{s}k_i l\mathrm{ch}k_i l+\mathrm{c}k_i l\mathrm{sh}k_i l}{1+\mathrm{c}k_i l\mathrm{ch}k_i l} \tag{B.4}$$

$$\psi_i(h) = \left\{m\left(1-\frac{C_i}{1-D_i}\right)+\rho_0\int_0^l F_i(y)\left[F_i(y)-\frac{C_i}{1-D_i}\right]\mathrm{d}y\right\}^{-1/2} \tag{B.5}$$

where $c \triangleq \cos$, $s \triangleq \sin$, $ch \triangleq \cosh$ and $sh \triangleq \sinh$.